Oligomeric oxidovanadium(IV) phosphates as a promising alternative to cobalt-based driers and accelerators.

Tomáš Foltýn,[a] Eliška Matušková,[a] David Rubeš,[a] Jaromír Vinklárek,[b] Miroslava Litecká,[c] Anna Krejčová,[d] and Jan Honzíček [a,*]

[a] Institute of Chemistry and Technology of Macromolecular Materials, Faculty of Chemical Technology, University of Pardubice, Studentská 573, 532 10 Pardubice, Czech Republic.

[b] Department of General and Inorganic Chemistry, Faculty of Chemical Technology, University of Pardubice, Studentská 573, 532 10 Pardubice, Czech Republic.

[c] Department of Materials Chemistry, Institute of Inorganic Chemistry of the CAS, Husinec-Řež 1001, 25068 Řež, Czech Republic.

[d] Institute of Environmental and Chemical Engineering, Faculty of Chemical Technology, University of Pardubice, Studentská 573, 532 10 Pardubice, Czech Republic.

* E-mail address: jan.honzicek@upce.cz (J. Honzíček).

Abstract:

This study reports promising catalytic activity of oxidovanadium(IV) dialkyl phosphates those can serve as primary driers for air-drying paints and as accelerators for room-temperature curing of unsaturated polyester resins. It describes an improved synthetic protocol giving title compounds at high yields and clarifies their molecular structure. The behavior in solution and in formulation of alkyd resin was investigated by electron paramagnetic resonance. Strong catalytic activity is documented by standard tests on several commercial alkyd binders and one multipurpose unsaturated polyester resin.

Keywords: Autoxidation; vanadium; primary drier; alkyd resin; unsaturated polyester; cobalt replacement

Highlights:

- Vanadium-based drier/accelerator synthesized and fully characterized
- Catalytic activity in alkyd resins and unsaturated polyesters established
- Cured films showing promising mechanical properties
- Example of cobalt-free technology reported

Graphical abstract:

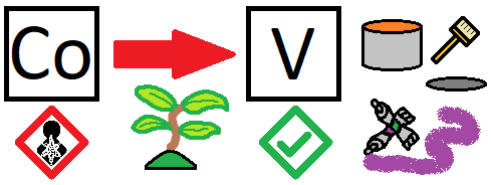

1. Introduction

The ongoing pressure on the reduction of cobalt exposure is driven by health risks [1,2]. Cobalt is generally considered an essential trace element for humans, playing a vital role as a component of the

vitamin B12 molecule, but its recommended daily income is extremely low (a few of μg) [3] and extensive exposure is associated with adverse effects on major organs and neurological damage [1,4]. In addition, soluble cobalt compounds have been classified as reproductive toxicants by the Cobalt REACH Consortium and the Cobalt Institute, which stimulates research on field cobalt-free technologies [5]. It should be noted that the replacement of cobalt-based technologies is further stimulated by the fluctuating price of cobalt due to production in areas blighted by conflicts [6]. Furthermore, a global deficiency of cobalt is expected to occur in the near future due to the growing demand for lithium ion batteries, where cobalt plays a key role [7].

Currently, cobalt carboxylates, soluble in organic solvents (e.g., cobalt 2-ethylhexanoate; **Co-2EH**), are widely used as primary driers for alkyd-based paints and inks [8,9] and as accelerators for room temperature curing of composites based on unsaturated polyester resins and vinyl esters [10].

In the field of alkyd resins, cobalt carboxylates serve as dual functional catalysts. They initiate the peroxidation of unsaturated fatty acid tails of the binder and accelerate the decomposition of the hydroperoxide intermediates. Crosslinks, responsible for the transformation of a liquid layer to a durable coating, are then formed by the addition of the peroxyl and alkoxyl radicals to double bonds and by recombination reactions [9].

The first generation of commercial cobalt-free systems involves manganese carboxylates and their mixtures with *N,N-chelating* ligands (e.g., bipyridine) [11]. These systems are commercially available, but have low activity under adverse climatic conditions and undesirable coloration of coating films [9]. Recently released manganese species that appear after treatment of manganese carboxylate with 1,4,7-trimethyl-1,4,7-triazacyclononane (Me_3TACN), known under the Borchi Dragon trademark, [5,12,13] and the iron bispidine complex, known under the Borchi OXY-Coat trademark (**Fe-BOC**), [5,14] perform at unusually low concentrations compared to conventional primary driers, which can be explained by an unusual coordination sphere of metals mimicking active sites of metalloenzymes responsible for oxidation reactions [15]. We note that considerable attention has also been paid to isolated dinuclear manganese compound $[\{Mn(Me_3TACN)\}_2(\mu\text{-}O)_3][PF_6]_2$ [16-18] and modified iron bispidine complexes with increased solubility in organic solvents [19,20].

Promising drying characteristics are further reported in the research literature for manganese acetylacetonates [11,21,22], iron complexes with polydentate ligands [5,23], ferrocene derivatives bearing electron-withdrawing substituents [24,25] and photoactive iron compounds [26]. The field of vanadium-based primary driers has focused mainly on oxidovanadium(IV) carboxylates [27] and oxidovanadium(IV) acetylacetonates [28-30], oxidovanadium(V) dithiocarbamates [31] and oxidovanadium(IV) sulfonates [32,33].

In the field of composite manufacturing, cobalt carboxylates accelerate the decomposition of organic peroxides, initiating radical polymerization of unsaturated polyester resins and vinyl resins [34]. Cobalt-free accelerators, developed for room-temperature cure, involve various redox-active transition metal compounds [35]. Promising activity has been reported for the iron bispidine complex [10], oxidovanadium(IV) toluenesulfonate [10], and the mixture of copper compounds with amine ligands [36].

This study aimed to investigate oxidovanadium(IV) phosphates and their potential application as driers for alkyd paints and accelerators for unsaturated polyester resins. These compounds were chosen due to the promising catalytic activity reported in the patent literature [37-39] but detailed research is still lacking. In this paper, we focus on efficient synthesis from readily available raw materials and the clarification of their molecular structure. The catalytic activity of the compounds will be documented

by standardized tests on several alkyd binders and commercial multipurpose unsaturated polyester resin.

2. Experimental Section

2.1 Materials

Vanadium(V) oxide, dibutyl phosphate, and bis(2-ethylhexyl) phosphate were purchased from Acros Organics. Acetone, methanol, ethanol, diethyl ether, tetrahydrofuran, hexane, and toluene were purchased from Penta. All compounds were used as obtained without further purification. Syntheses and purification processes were carried out in an air atmosphere.

The alkyd resins ChS-Alkyd S 471 X 60 (**S471**; OL = 47% soybean, AV = 6 mg KOH/g, nonvolatile content = 59.6%), ChS-Alkyd S 622 N 60 (**S622**; OL = 62% soybean, AV = 7 mg KOH/g, nonvolatile content = 58.4%), ChS-Alkyd TI 870 (**TI870**; OL = 87% TOFA, AV = 8 mg KOH/g, nonvolatile content = 98.6%) were obtained from Spolchemie. WorléeKyd B 850 U (**B850U**; OL = 45%, modified with urethane, AV = 15 mg KOH/g; 50%) was obtained from Worlée. Ekonal 1770 SFA 80 WS (**E1770**; OL = 70% TOFA, AV = 8 mg KOH/g; 80%) was obtained from Ekon. Unsaturated polyester ChS-Polyester 109 (**PES109**; 60 wt.% in styrene) was supplied from Stachema (Kolín, Czech Republic).

Cobalt(II) 2-ethylhexanoate (**Co-2EH**; in mineral spirits, 11 wt.% of Co; Sigma-Aldrich) and Borchi OXY-Coat (**Fe-BOC**, in propane-1,2-diol, 0.09 wt.% of Fe; Borchers) were used as standard driers for the evaluation of catalytic activity. Butanone peroxide (**MEKP**; 32 % in mixture of dimethyl phthalate and diacetone alcohol) and cobalt(II) carboxylate (**Co-C**; in organic solvents, 4 wt% of Co) were supplied from Stachema (Kolín, Czech Republic). We note that metal concentrations in alkyd formulations are given in wt.% based on the dry matter of the binder, while concentrations in formulations of unsaturated polyester resins are given in wt.% based on the full binder, as the styrene diluent is incorporated into the cured product.

*2.2 Synthesis of oxidovanadium(IV) dibutyl phosphate (**VO-1**)*

A suspension of vanadium(V) oxide (5.0 g; 30 mmol) in a mixture of ethanol (90 mL) and distilled water (45 mL) was treated with dibutyl phosphate (22.5 g, 120 mmol) and heated under reflux for 24 h to give a dark emulsion. The aqueous phase was decanted and the remaining dark blue liquid was diluted with diethyl ether (150 mL). Insoluble impurities were filtered out, and the solvent was vacuum evaporated. The crude product was treated with a mixture of methanol (75 mL) and hexane (75 mL). The solution was washed with distilled water (3 × 250 mL). The volatiles were vacuum evaporated to give a final product as a viscous liquid, which crystallizes within several weeks. Yield: 23.3 g (89 %). Anal Calc. for $C_{48}H_{110}O_{28}P_6V_3$ (MW 1474.04): C, 39.11; H, 7.52. Found: C, 39.43; H, 7.88. ICP-OES (%): V, 10.32 (calc. 10.37); P, 12.56 (calc. 12.61).

*2.3 Synthesis of oxidovanadium(IV) 2-ethylhexyl phosphate (**VO-2**)*

A suspension of vanadium(V) oxide (5.0 g; 30 mmol) in a mixture of ethanol (90 mL) and distilled water (45 ml) was treated with bis(2-ethylhexyl) phosphate (34.9 g; 120 mmol) and heated under reflux for 3 days to give a dark emulsion. The aqueous phase was decanted and the remaining dark blue liquid was diluted with diethyl ether (150 mL). Insoluble impurities were filtered out. The volatiles were vacuum evaporated to give a final product as a viscous liquid, which crystallizes within several weeks. Yield: 42.9 g (92 %). Anal Calc. for $C_{96}H_{206}O_{28}P_6V_3$ (MW 2147.31): C, 53.70; H, 9.67. Found: C, 53.99; H, 10.04. ICP-OES (%): V, 6.73 (calc. 7.12); 8.67 (calc. 8.65).

2.4 Electron paramagnetic resonance

EPR spectra were collected on MiniScope MS 300 and MiniScope 5000 spectrometers (Magnettech) in the microwave X-band (~9.5 GHz). The solution spectra were measured in sealed glass 50 µL-capillaries (Ringcaps, Hirchmann) or quartz tubes (ID = 5 mm) at 293 K. Solid samples were measured in quartz tubes (ID = 6 mm) at 293 K.

2.5 X-ray crystallography

Blue plate-shaped single crystals of **VO-1** were obtained by slow crystallization of a neat sample. Data were collected on a Rigaku XtaLAB Synergy S diffractometer equipped with micro-focus CuKα radiation and a Hybrid Pixel Array Detector (HyPix-6000HE). An Oxford Cryosystems (Cryostream 800) cooling device was used for data collection and crystals were kept at 100 K during data collection. The CrysAlisPro software [40] was used for data collection, cell refinement, and data reduction. Data were corrected for absorption effects using empirical absorption correction (spherical harmonics), implemented in SCALE3 ABSPACK scaling algorithm and numerical absorption correction based on gaussian integration over a multifaceted crystal model. Using Olex2 [41], the structure was solved with the SHELXT [42] structure solution program using intrinsic phasing and refined with the SHELXL [43] refinement package using least squares minimization. Most hydrogen atom positions were calculated geometrically and refined using the riding model, but some hydrogen atoms were refined freely. CCDC-2310820 contains the supplementary crystallographic data for this paper. These data can be obtained free of charge from The Cambridge Crystallographic Data Centre via www.ccdc.cam.ac.uk/data_request/cif.

2.6 Preparation of alkyd formulations

The alkyd resin (5 g) was treated with the given drier. The formulation was homogenized for 2 min and ultrasound sonicated for 3 min to remove air bubbles and then immediately used. In the case of the solvent-free binder **TI870**, the viscosity of the formulation was reduced by dilution to a solid content of 90 wt.% by dearomatized white spirit.

2.7 Drying time measurements

The drying times of the alkyd formulations were determined using the Beck-Koller method according to ASTM D5895 [44] using a Drying Time Recorder BK3 (TQC, Germany) in 24 h mode under standard laboratory conditions (T = 23°C, RH = 50%). The alkyd resin formulations were cast on glass strips (305 × 25 × 2 mm^3) using a frame applicator (76 µm-gap). Drying times are defined as follows: τ_1 = set-to-touch time, τ_2 = tack-free time, τ_3 = dry-hard time, τ_4 = dry-through time.

2.8 Preparation of unsaturated polyester resin formulations

Polyester resin **PES109** (20 g) was treated with a given accelerator and homogenized in a SpeedMixer DAC 150.3 FVZ (Hamm, Germany) at 3500 rpm for 2 min. After MEKP (169 µL) was added, the formulation was stirred mechanically with a glass rod for 30 s and degassed in a centrifuge (4000 rpm) for 2 min.

2.9 Gelation time measurements

The gelation time of the **PES109** formulations was determined on a Gelation Timer GT-5 (Cole-Parmer, Great Britain) with a 22 mm-stainless steel plunger according to ISO 2535 [45].

2.10 Exothermic behavior

The prepared formulations of unsaturated polyesters were inserted into a thermally isolated system. The development of temperature in the central part of the formulation was followed by a K-type

thermocouple temperature sensor (T_{99} = 7 s) using a multifunctional data logger Testo 435 (Testo, Lenzkirch, Germany). Measurements were made and data were processed according to our previous studies [10,46].

2.11 Relative hardness measurements

The hardness of the alkyd films was determined by Persoz method according to ISO 1522 [47] using a Pendulum Hardness Tester (Elcometer, UK) under standard laboratory conditions (T = 23°C, RH = 50%). The formulations were cast on glass plates (200 × 100 × 4 mm^3) using frame applicators of 90 µm-gap (**TI870**) and 150 µm-gap (**S471**, **S622**, **B850U**, **E1770**). The hardness of the **PES109** films was determined by the König method according to ISO 1522 [47] using a Pendulum Hardness Tester (BYK) under standard laboratory conditions (T = 23°C, RH = 50%). The formulations were cast on glass plates (200 × 100 × 4 mm^3) using frame applicators of 150 µm-gap, cured at room temperature for 24 h and post-cured in an oven for at 50°C for 1 h, 70°C for 1 h and 90°C for 1 h.

2.12 Measurements of film coloration

The coloration of the transparent films was measured on an RM200QC colorimeter (X-Rite). It is expressed in the CIELAB color space with a standard illuminant D65 and an observer at 10°. Measurements were made on coated glass plates (used before for measurements of relative hardness) on a white underlay 100 days after casting. Data are given as averaged values obtained from ten different spots on the coating.

2.13 Measurements of film thickness

The thickness of dry coatings was determined using a modified Roughness Meter TQC-SP1560 (TQC) according to ISO 2808:2007 [48].

2.14 Measurements of solvent resistance and adhesion

Resistance test to butanone (MEK) was performed according to ASTM D 4752 [49] using a cotton swab, dipped in MEK every 20 s. The swab was rubbed onto the surface of the coating until the substate was exposed. The adhesion to the coating was determined by cross-cut test according to ASTM D 3359 [50] using the Zehntner cross-cut device. Both tests were performed on coated glass plates (used before for measurements of relative hardness) 100 days after casting.

2.15 Measurements of tensile properties

Alkyd resin formulations were cast on Teflon plates with an applicator of 250 µm-gap. After 45 days of curing, the coatings were removed and dog-bone-shaped specimens (70 µm thickness, 47.5 mm total length, 14.7 mm wide gripping area, and 12.5 × 5 mm^2 thinned middle section dimensions) were cut by punch. Tensile testing was performed on an Instron 1122 universal testing machine (Bluehill Universal) with a head span of 30 mm at a head speed of 5 mm/min according to ASTM D1708-18 [51].

2.16 Dynamic mechanical analysis (DMA)

The **PES109** formulations were poured into silicone molds, cured at room temperature overnight and post-cured in an oven at 50°C for 1 h, 70°C for 1 h and 90°C for 1 h. The samples were slowly cooled to ambient temperature to avoid thermal stress. Measurements were made in blocks (50 × 6 × 3 mm^3) using a DX045 device (RMI) in a single fixed point cantilever configuration with a span between clamps of 11 mm, a deviation of ± 0.15 mm and a frequency of 1 Hz. Measurements were carried out in the range of –60°C to 250°C and with a heating rate of 3°C/min.

2.17 Measurements of flexural properties

Flexural testing was conducted on **PES109** specimens of the same shape as that used for DMA. Measurements were made on a universal testing machine Autograph AGS-X 50kN (Shimadzu) in a three-point bending configuration with a support span of 40 mm at a head speed of 1 mm/min according to ISO 178:2019 [52]. The experiment was stopped when the specimen ruptured or the force exerted on the specimen was below 10 N.

2.18 Impact toughness

The measurements were conducted according to Charpy on **PES109** specimens of the same shape as that used for DMA (unnotched specimens). The test was carried out on a Plastic Pendulum Impact Tester 501 J-3 (Shenzhen Wance Testing Machine) with a support span of 40 mm according to ČSN 64 0612 [53].

2.19 Gel content

The post-cured samples of **PES109** (same shape as used for DMA) were grinded in an IKA A10 Basic impact mill for 2 min. The ground resin was weighed (m_1), treated with THF and stirred in closed vessels for 24 h. The solid content was filtered, washed with THF, dried in an oven at 50°C until a constant weight (m_2). The gel content was calculated as (m_2/m_1) × 100.

2.20 Plasma-optical emission spectroscopy

The phosphate and vanadium contents were determined using inductively coupled plasma-optical emission spectroscopy (ICP OES). Samples were decomposed in a Speedwave Xpert microwave mineralizer (Berghof, Tübingen, Germany). They were precisely weighed (~0.05 g), treated with nitric acid (7 mL) and allowed to react for 20 min in an open vessel before being decomposed (175 °C for 15 min, 220 °C for 25 min). The mineralized sample was then diluted to a final volume of 25 mL. The elemental analysis was performed with the sequential, radially viewed ICP OES spectrometer INTEGRA 6000 (GBC, Dandenong, Australia), equipped with the concentric nebulizer and the glass cyclonic spray chamber (both Glass Expansion, Australia). Spectral lines of P at 214.914 nm and V at 311.071 nm were used. The operation conditions of the ICP-OES analysis: sample flow rate = 1.5 mL/min, plasma power = 1000 W. The calibration standards were prepared using a commercially available stock standard solution of P and V, both containing 1 g/L (SCP, Baie D'Urfé, Canada).

2.21 Infrared spectroscopy

Time-resolved spectra in the mid-infrared region (4000–400 cm^{-1}) were collected on a Nicolet iS50 FTIR spectrometer using the attenuated total reflection (ATR) sampling technique (64 scans per spectrum, data spacing = 0.5 cm^{-1}). The alkyd formulations were applied on a built-in diamond ATR crystal using a frame applicator of 25 µm gap. It gives coatings of 5 µm wet thickness as the crystal surface lies 20 µm above the plate, on which formulations are cast. Spectra were recorded every 5 min for 24 h under standard conditions (T = 23 °C; RH = 50%). Data processing was carried out according to our previous studies [54].

3. Results and Discussion

3.1 Synthesis and characterization

Oxidovanadium(IV) phosphates can be prepared by a reaction of oxidovanadium(V) isopropoxide with alkyl phosphates [55] or by extraction of aqueous solution of oxidovanadium(IV) sulfate with dialkyl phosphate [56]. Related phosphinate complexes are accessible from oxidovanadium(IV) acetylacetonate and dialkylphosphinic acid [57,58].

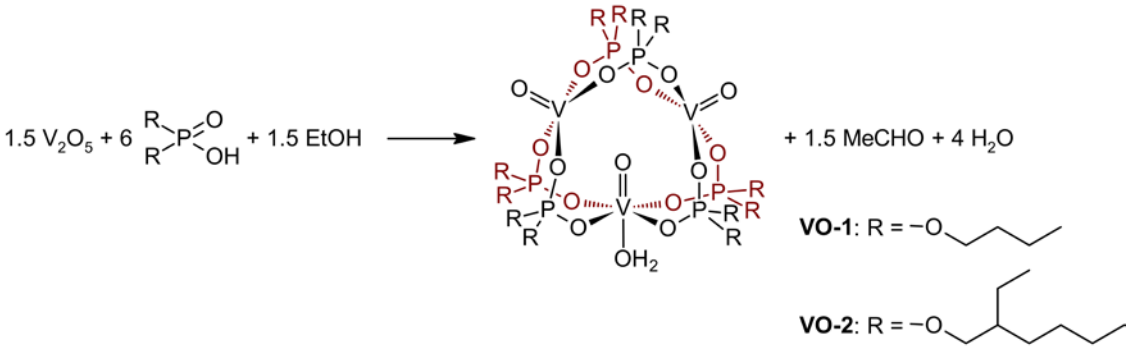

Scheme 1. Synthesis of oxidovanadium(IV) phosphates.

To simplify the synthetic protocol and reduce costs, a direct reaction of vanadium(V) oxide with dialkyl phosphates was investigated. It was revealed that the reaction proceeds in aqueous ethanol at elevated temperature according to Scheme 1. Surprisingly, no additional strong acid is necessary to reduce vanadium from the oxidation state V to the IV. Acetaldehyde, which appears upon ethanol oxidation, can be easily distilled off upon heating the reaction mixture. We note that the reaction is accompanied by a color change from yellowish-brown to deep blue, and the appearance of a two-phase system. The organic phase, which contains the main product, can be diluted with diethyl ether and purified by filtration. When an excess of vanadium(V) oxide is used, the final products $[(VO)_2\{VO(OH_2)\}\{\mu\text{-}O_2P(OR)_2\}_6]$ (**VO-1**: R = Et, **VO-2**: R = 2-ethylhexyl) of satisfactory purity were obtained after solvent evaporation. The vanadium and phosphorus content in the samples of **1** and **2** was verified by IPC analysis (Table S2 in Supporting Information).

Compound **1** appears as a blue high-viscous liquid that undergoes very slow crystallization. The large crystals obtained are well soluble in a variety of organic solvents, including nonpolar solvents (hexane, toluene, xylene), ethers (Et_2O, THF), chlorinated solvents (CH_2Cl_2, $CHCl_3$), alcohols (MeOH, EtOH) and acetone. The compound **VO-2** appears as a blue solid of lower solubility.

Solutions of **VO-1** and **VO-2** in non-coordinating solvents (e.g., hydrocarbons, chlorinated hydrocarbons) and Et_2O give a 22-line EPR spectrum with equally spaced resonances superposed on a broad single band (Figure 1, Table 1). The 22-line spectrum is typical for dissolved species containing three magnetically equivalent vanadium(IV) atoms, whereas the broad band implies the presence of colloid particles.

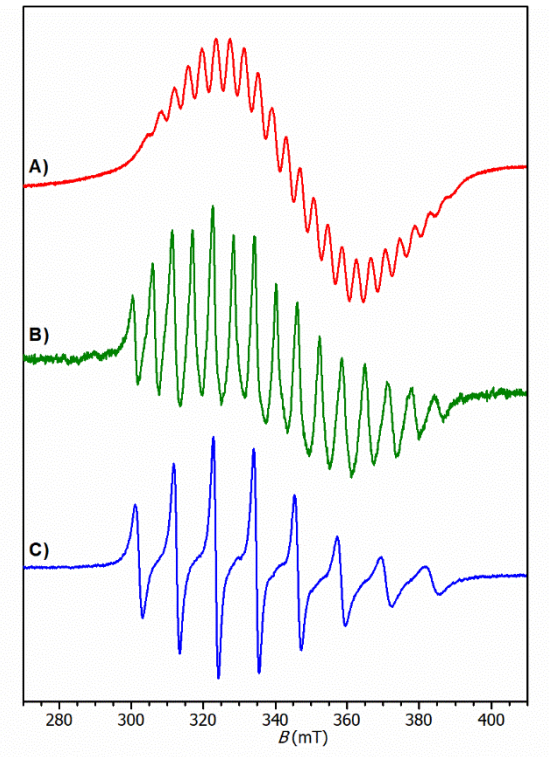

Figure 1. EPR spectra of **VO-1** solutions in a) diethyl ether, b) tetrahydrofuran, and c) methanol.

Table 1. EPR data of vanadium complexes.

		$\lvert A_{iso} \rvert$ (mT)	g_{iso}	N [a]	n [b]
VO-1	Et_2O	3.93	1.954	22	3
VO-1	THF	6.02	1.963	15	2
VO-1	MeOH	11.62	1.964	8	1
VO-2	Et_2O	4.02	1.955	22	3
VO-2	THF	6.07	1.961	15	2
VO-2	MeOH	11.55	1.966	8	1

[a] number of lines in the EPR spectrum. [a] number of vanadium atoms in the complex.

The proposed molecular structure of the compound **VO-1** was confirmed by X-ray diffraction analysis on a single crystal. The observed oligomeric species contain three oxidovanadium(IV) units connected by six bridging phosphate ligands (Figure 2). The vanadium atoms in the oligomeric cage are not equivalent, as only two of them are pentacoordinated with the oxido ligand directed out of the cage. The third vanadium atom is hexacoordinated, since the sixth position is occupied by the aqua ligand with a V–O bond length of 2.2156(17) Å. In this case, the oxido ligand (O1) is directed to the cage. This rather unusual oligomeric cage is probably stabilized by the weak interactions V2···O1 (2.9194(17) Å) and V3···O1 (2.8248(14) Å), as previously implied for isostructural compounds $[(VO)_2\{VO(NCMe)\}\{\mu\text{-}O_2P(OEt)_2\}_6]$ [55], $[(VO)_2\{VO(L)\}\{\mu\text{-}O_2P(Bn)_2\}_6]$ (L = H_2O, py) [57]. This interpretation is supported by the prolongation of the double bond V1=O1 (1.6082(15) Å) compared to V2=O2 (1.5811(17) Å) and V3=O3 (1.5794(16) Å).

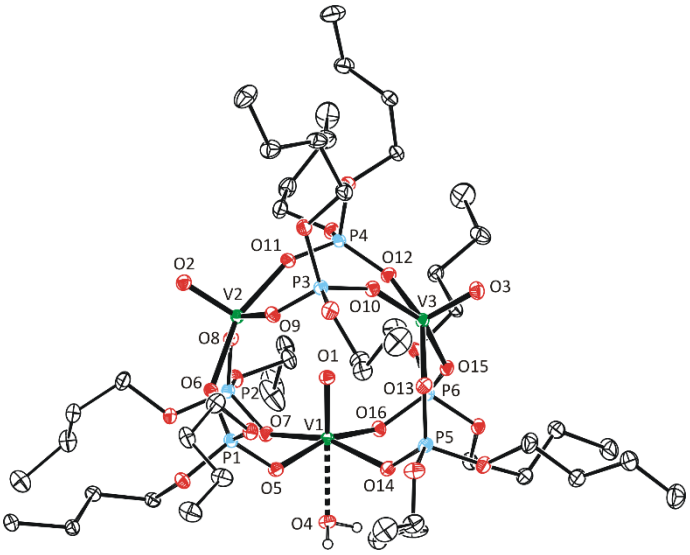

Figure 2. Molecular structure of **VO-1**. Thermal ellipsoids set to 30% probability. Only one position of disordered alkyl moieties is shown for clarity.

Trinuclear species **VO-1** and **VO-2** are long-term stable in hydrocarbons and Et_2O. The slow decomposition in THF is attributed to trace contamination with peroxides. The decomposition process was followed by EPR spectroscopy. Appeared 15-line spectrum with equally spaced resonances imply the formation of a dinuclear species, in which one vanadium atom is probably oxidized (Figure 1, Table 1). It should be noted that the same species is easily generated in Et_2O solution when treated with hydrogen peroxide, which supports our suggestion that oxidation of one vanadium atom is necessary for generation of dinuclear species.

Our EPR measurements further show that the compound **VO-1** is unstable in methanol and EtOH. It undergoes immediate splitting to a mononuclear vanadium(IV) species, as documented by the observed 8-line EPR spectrum (Figure 1). In this case, participation of the redox process is not expected, as it proceeds rapidly even under an inert atmosphere of nitrogen.

3.2 Catalytic activity in air-drying paints

Preliminary catalytic activity tests were performed on medium-oil-length alkyd resin modified with soybean oil **S471**. The drying times collected for the formulations of **VO-1** and **VO-2** were compared with those obtained for the cobalt-based drier **Co-2EH** and its commercial iron-based alternative **Fe-BOC**. The effect of the driers on alkyd drying and hardening is shown in Figure 3 and Table S3 in the Supporting Information.

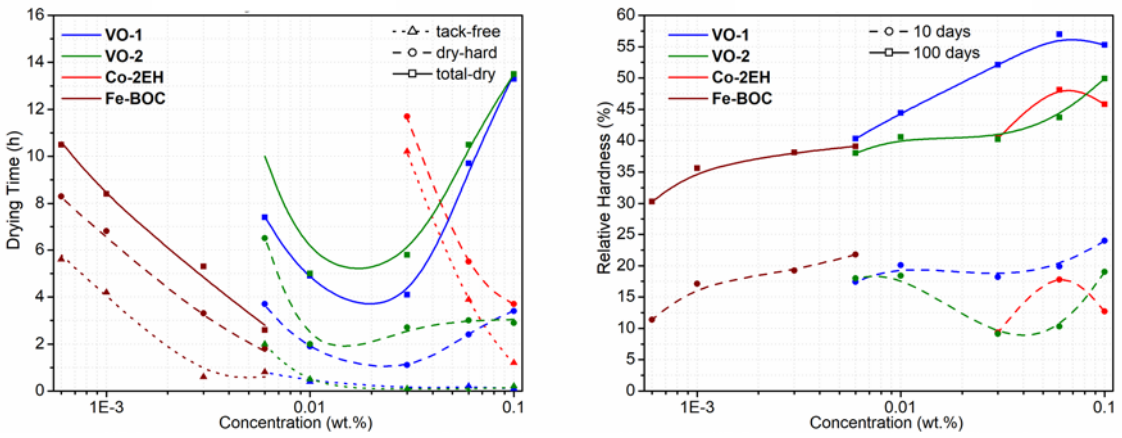

Figure 3. Drying times (left) and relative hardness (right) of formulations of solvent-borne alkyd **S471** treated with different primary driers.

Vanadium-based driers **VO-1** and **VO-2** show high activity in the binder **S471**. The optimal dosage, estimated as a minimum on the dry-hard and total-dry times curves (T_3 and T_4), stays between 0.01 and 0.03 wt.% of the metal in the dry matter content. At higher concentrations, a strong overdose effect was observed. It is documented by the considerable prolongation of the dry-hard time (T_3) and the total-dry time (T_4). Our measurements show that the compound **VO-1** gives, at a given concentration, considerably shorter drying times than **VO-2**. Its higher activity is further evidenced by measurements of the relative hardness of the cured films. Hence, **VO-1** gives films that are much harder than **VO-2.** At 0.06 wt.%, it reaches a final hardness ($H_{rel,100d}$) of 57.0%.

The cobalt-based drier **Co-2EH** is active at higher concentrations than **VO-1** and **VO-2**. Short tack-free times (T_2) and dry-hard times (T_3) were observed in the range 0.06 to 0.1 wt.% of metal in the dry matter content, which corresponds to the dose recommended by the suppliers. However, **Co-2EH** treated coatings are not dried completely within 24 h, as documented by the total drying time values (see T_4 in Table S3 in Supporting Information). We note that cobalt-based driers are recommended to be used in combination with secondary driers that improve through drying of alkyd formulations [9]. Films treated with **Co-2EH** show high final hardness ($H_{rel,100d}$), but do not reach the values obtained for **VO-1** at a given concentration.

The commercial iron-based drier **Fe-BOC** is active in considerably lower doses than the other driers under study. Acceptable tack-free, dry-hard, and total-dry times are obtained already at 1×10^{-3} wt.% of metal in dry matter content. Optimal performance was observed at 6×10^{-3} wt.%, where the film was completely dry within 2.6 h. After 10 days of curing, films treated with **Fe-BOC** (1×10^{-3} to 6×10^{-3} wt.%) show a similar hardness as those treated with **VO-1** (0.06 wt.%). However, the long-term activity of **Fe-BOC** is much lower, as documented by the lower final hardness ($H_{rel,100d}$).

Further testing was carried out only on the more promising derivative **VO-1**, as it shows a higher solubility in organic solvents and a higher activity in the binder **S471**. The higher vanadium content is also favorable for suggested application. We note that both commercial driers (**Co-2EH** and **Fe-BOC**) were used as benchmarks for further testing, as they exhibit very different drying performance in **S471**.

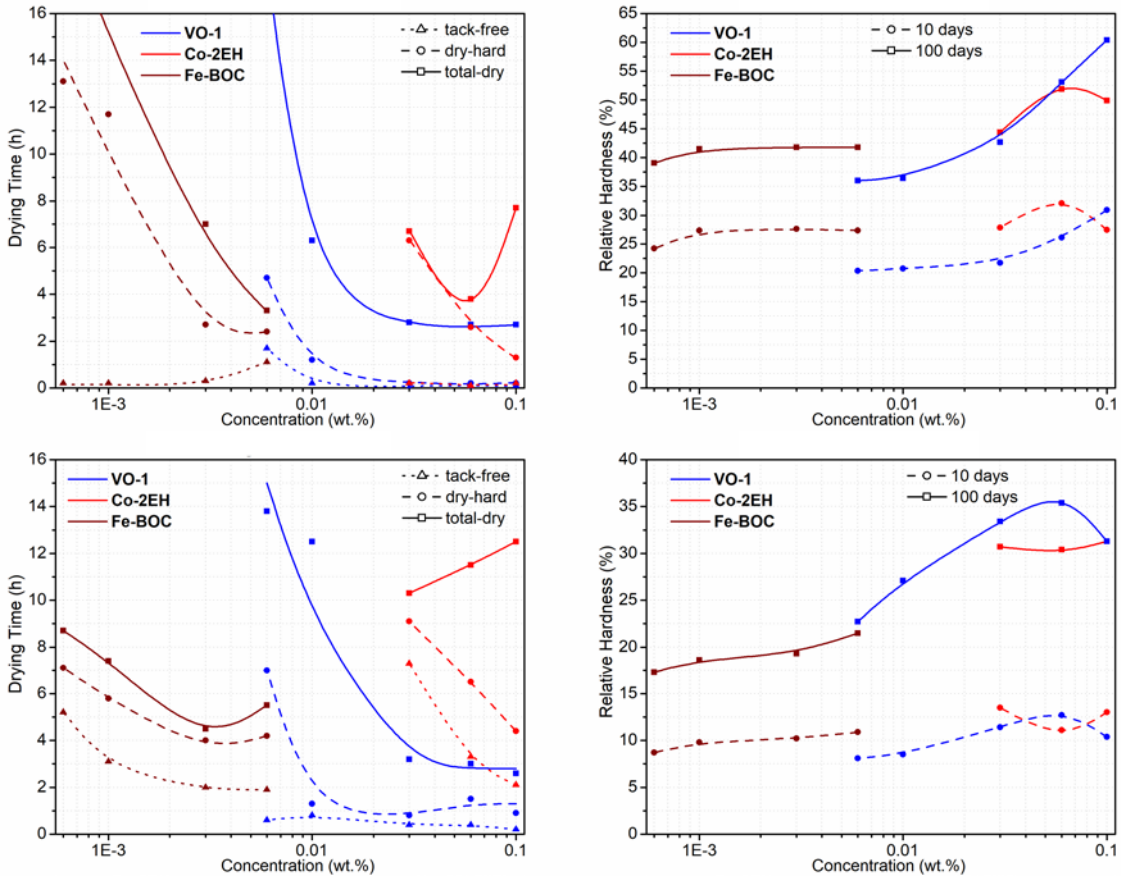

Figure 4. Drying times (left) and relative hardness (right) of formulations of solvent-borne alkyds **B850U** (top) and **S622** (bottom) treated with different primary driers.

Further catalytic activity tests were performed on the medium-oil-length urethane alkyd resin **B850U** and the long-oil-length alkyd resin modified with soybean oil **S622**. The results of the tests are given in Figure 4 and Tables S4 and S5 in the Supporting Information. In both binders, **VO-1** exhibits high catalytic activity in the range of concentrations 0.03 to 0.1 wt.%, where the tack-free time (T_2) does not exceed 0.4 h and the total-dry time (T_4) 3.2 h. The cobalt-based drier **Co-2EH** is more sensitive to dosage. In **B850U**, it shows optimal performance at 0.06 wt.% and a higher concentration leads to prolongation of the total-dry time (T_3). The **Co-2EH** /**S622** formulation exhibits slow though drying, as is evident from the increasing value of the total-dry time (T_4) with increasing concentration. The iron-based drier **Fe-BOC** shows high activity in both binders. In **B850U**, good performance was observed in the concentration range of 3×10^{-3} to 6×10^{-3} wt.%, where the total-dry time does not exceed 7.0 h. In **S622**, the iron-based drier is applicable in a wider range 1×10^{-3} to 6×10^{-3} wt.%.

The relative hardness of the films treated with **VO-1** and **Co-2EH** is comparable. In the case of **Co-2EH**, a faster increase in hardness is observed within the first ten days. However, in a proper dose, **VO-1** allows achieving a higher final hardness ($H_{rel,100d}$). We note that the final hardness of films treated with **Fe-BOC** is much lower than in the case of **VO-1** and **Co-2EH** when comparing performance at optimal concentrations.

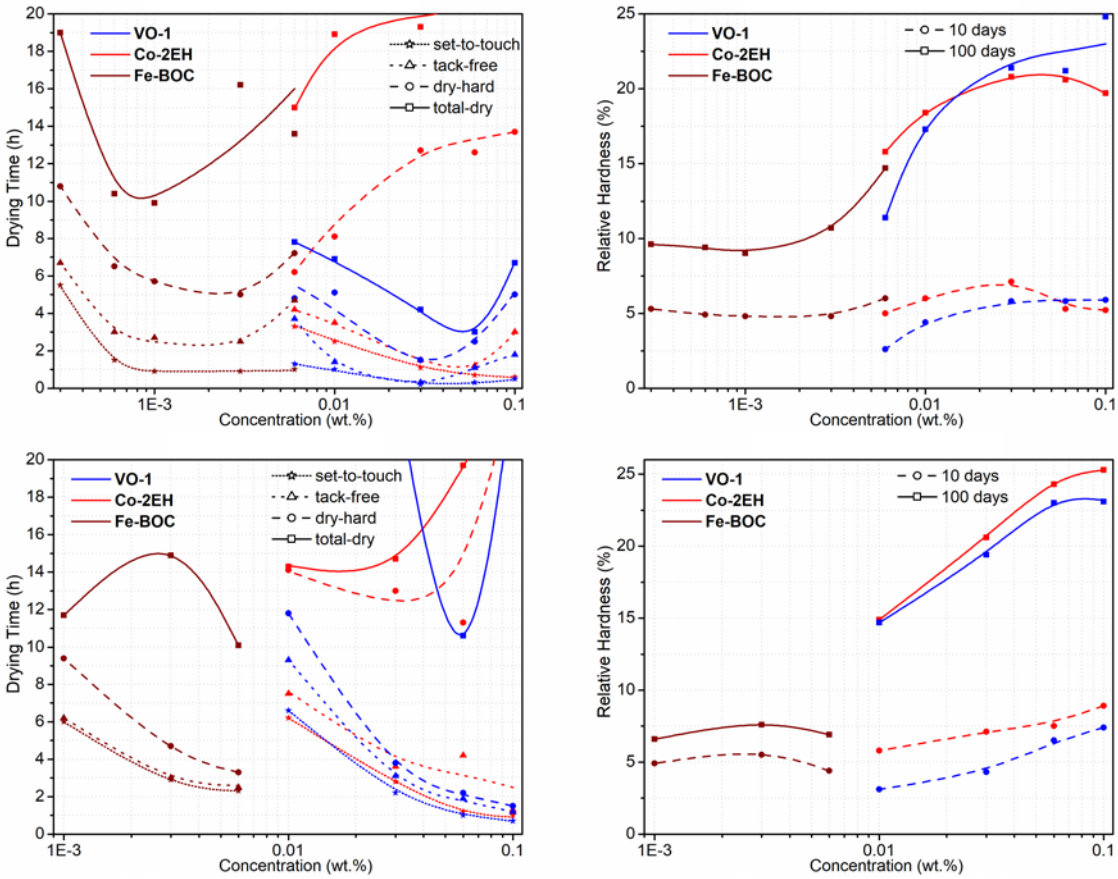

Figure 5. Drying times (left) and relative hardness (right) of formulations of high-solid alkyds **E1770** (top) and **TI870** (bottom) treated with different primary driers.

Two high-solid alkyd resins were chosen for final testing, namely the **E1770** and **TI870** binders. Both resins are modified with tall oil fatty acids. In **E1770**, the vanadium-based drier exhibits very good performance in the range of 0.006 to 0.1 wt.%. Short total-dry times (T_4), not exceeding 7.8 h, document good through drying without the need for secondary driers (Figure 5 and Tables S6 and S7 in Supporting Information). Considerably higher T_4 values were obtained for the cobalt- and iron-based benchmarks. The dependence of relative hardness on concentration is similar for **VO-1** and **Co-2EH**. At high doses, both driers give films of much higher final hardness ($H_{rel,100d}$) than observed for **Fe-BOC**.

The **TI870** binder has a much stronger tendency to non-homogeneous drying, as verified by our measurements. Films cured with **VO-1** were not completely dry within 24 h except for 0.06 wt.% concentration. Nevertheless, the drier is highly active in the range of 0.03 to 0.1 wt.%, as is evident from the short dry-hard times (T_3) not exceeding 3.8 h. The very slow through drying of films treated with **Co-2EH** is documented by much higher T_3 values, although the tack-free times (T_2) are short. At optimal doses, **Fe-BOC** behavior resembles that of **VO-1**, as documented by similar drying times. Nevertheless, films treated with **VO-1** exhibit a much higher final hardness ($H_{rel,100d}$), close to the values obtained for **Co-2EH**.

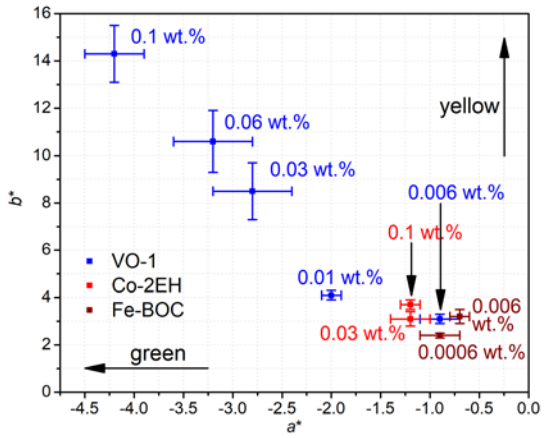

Figure 6. Coloration in **S471** films treated with different driers. Only the upper and lower limit concentrations of **Co-2EH** and **Fe-BOC** are given for clarity. Wet film thickness = 250 µm.

3.3 Coloration of alkyd films

The effect of **VO-1** drier on the discoloration of alkyd films was studied on transparent samples cured at room temperature for 100 days. Figure 6 shows the color change in the CIELAB space for the **S471** formulations, which was taken as a representative example. Full data for a wider series of alkyd resins are given in the Supporting Information.

Films treated with a high dose of **VO-1** turn greenish yellow. At 0.1 wt.%, the effect is clearly visible to the eye, since the shift in the a^* and b^* axes is –4.2 ± 0.3 and 14.3 ± 1.2, respectively. The drop in perceptual lightness is small; L^* = 98.0 ± 0.3. Lowering the drier concentration considerably reduces the effect of discoloration. At 0.01 wt.%, it is hardly perceivable from other driers under the study. In the case of commercial driers (**Co-2EH** and **Fe-BOC**), the effect on film coloration is low. At lower concentration limits, it is given by the alkyd binder itself. We note that films without a drier could not be used as standard as they have surface defects.

The behavior of the driers in the other alkyds is very similar to that of the formulations of **S471**. The difference in absolute values of the given binders is due to the coloration of the binders themselves.

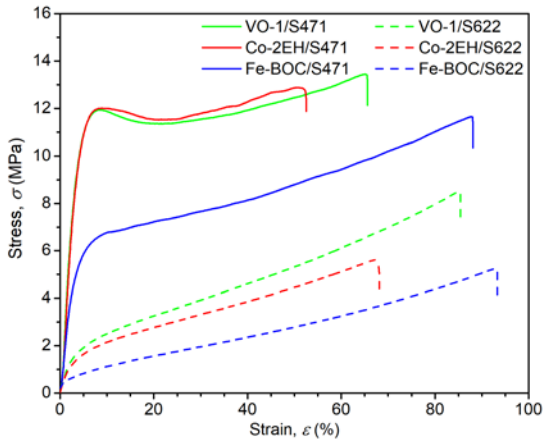

Figure 7. Tensile stress-strain diagrams of cured films of alkyd resins **S471** and **S622**.

Table 2. Tensile properties of alkyd films.

Drier	Binder	σ_{max} (MPa)	ε_f (%)	E (MPa)	σ_{UYP} (MPa)
VO-1	**S471**	13.8 ± 1.0	65.8 ± 9.3	412 ± 37	11.7 ± 0.9
Co	**S471**	12.6 ± 1.0	54.6 ± 10.5	399 ± 40	11.5 ± 0.7
Fe-BOC	**S471**	11.2 ± 1.2	92.9 ± 11.4	202 ± 22	– [a]
VO-1	**S622**	7.3 ± 1.3	86.6 ± 13.3	56 ± 16	– [a]
Co	**S622**	5.6 ± 1.0	68.2 ± 10.0	61 ± 12	– [a]
Fe-BOC	**S622**	5.2 ± 1.1	94.6 ± 13.8	34 ± 10	– [a]

[a] Upper yield point not observed.

3.4 Mechanical properties of the cured films

The effect of the driers on the mechanical properties of was studied in formulations of **S471** and **S622** treated with **VO-1** (0.1 wt.%), **Co** (0.1 wt.%) and **Fe-BOC** (1×10^{-3} wt.%) cured at room temperature for 30 days (Table 2, Figure 7). The shape of the tensile stress-strain diagram implies that the film cured by **Co**/**S471** is in a glassy state at room temperature [59]. The stress (σ) increases with increasing strain (ε) linearly obeying Hooke's law until σ ~ 10 MPa (E = 394 ± 43 GPa). The elastic limit is reached at ~11.7 ± 0.9 MPa and the lower yield point at ~20% strain. Subsequently, the strain hardening occurs and the stress increases very slowly until failure at elongation (ε_f) of 54.6 ± 10.5% and stress (σ_{max}) of 12.6 ± 1.0 MPa. Samples treated with **VO-1** show very similar behavior, as documented in the stress-strain curve, shown in Figure 7, and virtually the same Young's modulus, elastic limit, and lower yield point (Table 2). However, the higher ductility of films treated with **VO-1**/**S471** is documented by a wider strain hardening region, as specimens break with significantly higher elongation (ε_f = 65.8 ± 9.3 %). Unlike **Co** and **VO-1**, the iron-based drier **Fe-BOC** gives films with much lower stiffness, as evidenced by the lower value of Young's modulus (E = 202 ± 22 MPa). A considerably lower proportionality limit (~ 5 MPa), absence of an upper yield point, together with failure at a considerably higher strain (ε_f = 92.9 ± 11.4%) imply a considerably lower T_g value for the **Fe-BOC**/**S471** film [59]. Such behavior is in line with the lower Persoz hardness mentioned above. It is probably caused by a higher elasticity of the polymeric chains due to a lower density of crosslinking.

The cured **S622** films give typical stress-strain diagrams for rubbery polymers [59], which is in line with the higher oil-length of the binder. Nevertheless, even in this case, variation of the mechanical properties is observed depending on the primary drier. Formulations treated with **Co** and **VO-1** exhibit a short linear region until σ ~1 MPa. Afterward, the films yield, and the stress rises with stain almost linearly until failure. In the case of the **Co/S622** formulation, the specimens break at σ_{max} = 5.6 ± 1.0 MPa and ε_f = 68.2 ± 10.0 %. The film treated with **VO-1** is more ductile, since it brakes at higher values (σ_{max} = 7.3 ± 1.3 MPa; ε_f = 86.6 ± 13.3). The lower stiffness of the **Fe-BOC/S622** film is evidenced by a very short linear region (until σ ~ 0.5 MPa) and a lower Young's modulus (34 ± 10 MPa). It breaks at higher strain than **VO-1/S622**, but it is less ductile due to considerably lower ultimate tensile toughness (σ_{max} = 5.2 ± 1.1 MPa). The higher elasticity of **Fe-BOC/S622** is ascribed to a lower density of crosslinking, documenting a lower long-term activity of the drier.

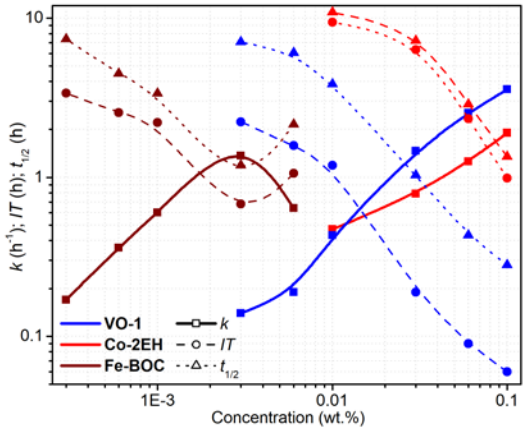

Figure 8. Rate coefficients (*k*) induction times (*IT*) and half-lives ($t_{1/2}$) for the formulation of the alkyd resin **S471** treated with different driers.

3.5 Kinetics of the autoxidation process

The curing of the alkyd formulations was followed by time-resolved infrared spectroscopy. The measurements were made in thin films of the **S471** binder treated with **VO-1**, **Co-2EH** and **Fe-BOC** driers according to the previously established protocol [54]. The development of the characteristic C–H stretching mode ν_a(*cis*-C=*C*–*H*), appearing at 3008 cm^{-1}, allows us to follow the first reaction step of the curing process consisting of peroxidation of the fatty acid tails [9]. The kinetic parameters, summarized in Figure 8, describe the behavior of thin films of ~5 µm wet thickness, which can be taken as a model for a surface of a common coating of higher thickness [54]. We note that plots following consumption of the reactive substrate together with the full list of kinetic data are given in Supporting Information.

The high activity of **VO-1** in the concentration range of 0.1–0.01 wt.% is documented by the high rate coefficient of the peroxidation reaction (*k*) and the very short induction times (*IT*). At a given concentration of **VO-1**, both parameters are superior compared to **Co-2EH**, leading to considerably shorter half-lives of the process ($t_{1/2}$). As expected, lowering the metal concentration leads to prolongation of *IT* while *k* decreases. Although the rate coefficient of **Co-2EH** decreases slower than in the case of **VO-1**, its performance deteriorates at 0.03 wt.% owing to the long induction time (*IT* = 6.33 h). The drier **Fe-BOC** shows optimal performance at 0.003 wt.%. Similarly, as in the case of **VO-1**, loss of catalytic activity at a lower dosage is due to low rate coefficients rather than long induction times. At higher doses, a decrease in *k* and a prolongation of *IT* are observed even in thin coatings, ruling out the effect of slow diffusion of dioxygen due to densely crosslinked skin. Presumably, too high concentration of radicals leads to increased recombination reactions in the early stages of the curing process. We note that the peroxidation process can also be affected by the propane-1,2-diol used in **Fe-BOC** as a solvent.

3.6 EPR spectra of the alkyd formulation

The fresh formulation of the **S471** resin treated with **VO-1** (0.1 wt.%) gives one broad band in the EPR spectrum without resolved hyperfine coupling. It implies the presence of colloid particles of the vanadium complex dispersed in the binder but not dissolved at the molecular level (Figure 9). Upon curing at room temperature, the hyperfine structure appears due to interaction of the unpaired electron with ^{51}V nuclei (*I* = 7/2, abundance = 99.8%). After 24 h of curing, the anisotropic spectrum of

one mononuclear vanadium(IV) species predominates ($A_{\parallel}$ = 19.35 mT, $A_{\perp}$ =7.30 mT, $g_{\parallel}$ = 1.93, $g_{\perp}$ = 1.975). It proves very slow dissociation of the colloid particles, which can proceed even in a crosslinked binder (dry-hard according to drying recorder testing). We note that the presence of the dissolved trinuclear species **VO-1** was evidenced in films cured for 0.5–8 h, as multiple bands in the region 300 to 310 mT.

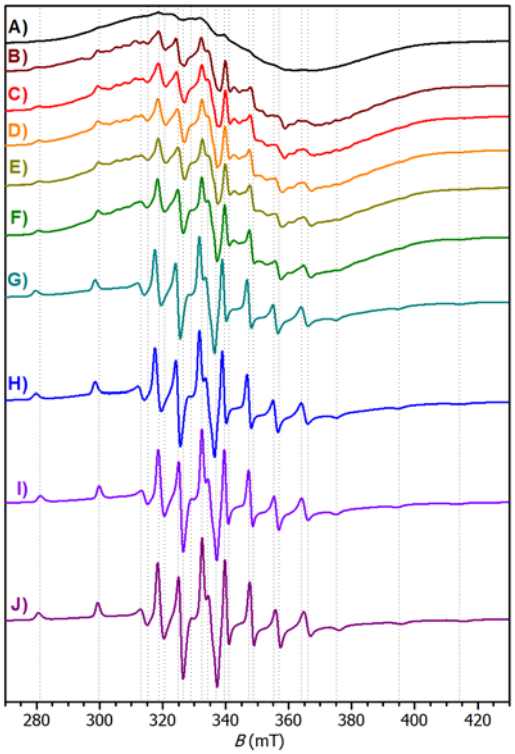

Figure 9. EPR spectra of fresh **VO-1** solution in alkyd resin **S471** at a dose of 0.1 wt.% (A) and films of the same formulation cured 30 min (B), 1 h (C), 2 h (D), 4 h (E), 8 h (F), 1 d (G), 2 d (H), 4 d (I) and 8 d (J).

3.7 Catalytic activity in unsaturated polyester resin

The acceleration effect of **VO-1** on the room temperature cure of the commercial unsaturated polyester resin **PES109** in combination with the butanone peroxide (**MEKP**) initiator was investigated under the conditions given in our previous study [10].

The compound **VO-1** exhibits high catalytic activity in the concentration range of 1×10^{-3} to 6×10^{-3} wt.%, as documented by gelation times (t_{gel}) in the range 5 to 40 min, which was arbitrarily defined as suitable for common applications. The effect of **VO-1** concentration on t_{gel} is shown in Figure 10 and is compared with the commercial benchmarks **Co-C** and **Fe-BOC**. It shows that the vanadium-based accelerator **VO-1** is active at considerably lower concentrations than **Co-C** but not at the same low concentrations as reported for **Fe-BOC** [10]. The main advantage of **VO-1** (over **Fe-BOC**) is the absence of an overdose effect that prolongs the t_{gel} at high doses.

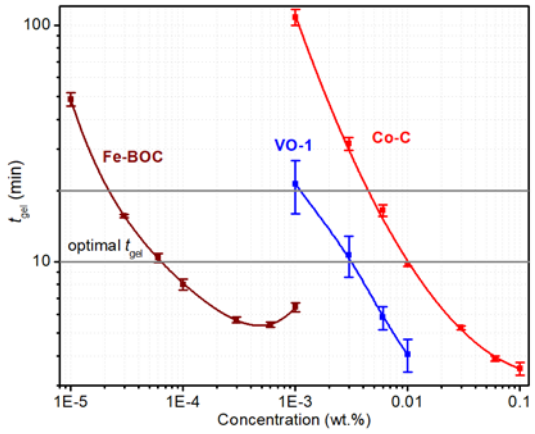

Figure 10. Effect of **VO-1** on the gelation time of unsaturated polyester. Data for **Co-C** and **Fe-BOC**, measured under the same conditions, are given for comparison [10].

Measurements of exothermic behavior in the thermally isolated assembly confirmed the high catalytic activity of **VO-1** at concentrations 3×10^{-3} to 0.03 wt.%, as documented in exothermic curves and their first derivatives, shown in Figure 11. In this concentration range, high values of the maximal rate of temperature rise $(dT/dt)_{max}$ are observed together with short times at which this maximum is obtained (t_{max}). The highest value of $(dT/dt)_{max}$ is reached at 0.01 wt.%. The lower value of $(dT/dt)_{max}$, observed at 0.03 wt.%, can be taken as the first sign of overdosing. An increased concentration leads to a considerable prolongation of t_{max}. The lower adiabatic temperature (T_{ad}), observed at 0.06 wt.%, implies premature decomposition of peroxide leading to a lower degree of cure. It should be noted that lowering the metal concentration to 1×10^{-3} wt.% leads to considerable prolongation of t_{max}, but the $(dT/dt)_{max}$ stays high (47.8 °C/min). A high value of T_{ad} implies a high degree of cure, comparable to formulations containing **VO-1** at a higher dose. We note that exothermic data for the **Co-C** and **Fe-BOC** benchmarks were published elsewhere [10]. They imply an increase in catalytic activity in the order of **Co-C** > **VO-1** > **Fe-BOC**.

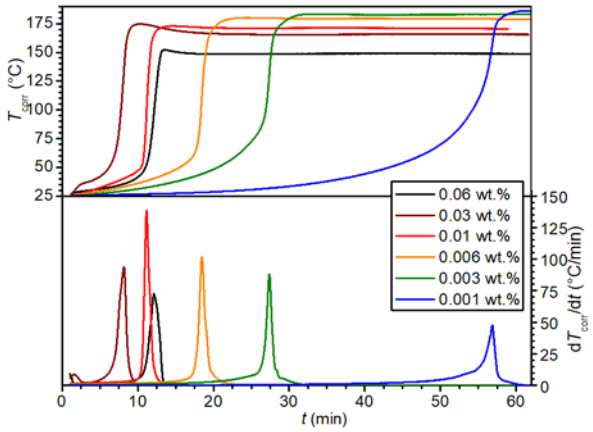

Figure 11. Effect of metal concentration on corrected exotherms and rate of temperature increase for unsaturated polyester treated with **VO-1**.

3.8 Mechanical properties of bulk polyester samples

Properties of cured polyester resin **PES109** were investigated on standard specimens prepared in silicone molds. Accelerators were dosed below the optimal range estimated by gelation time

measurements (**VO-1**: 6×10^{-4} wt.%; **Co-C**: 3×10^{-3} wt.%; **Fe-BOC**: 1×10^{-5} wt.%) due to premature increase in viscosity. We note that all samples were post-cured according to standard protocols to obtain reproducible data.

Extractions by THF revealed a high gel content for all samples in the study, which implies the appearance of a well crosslinked network. This conclusion is supported by the DMA analysis. The samples show a very similar shape of the DMA curves with a minor variation in the T_g value (Table 3). We note that all samples showed secondary peaks in the low temperature region (0 to 100°C) of the dumping factor curve (tan δ), assigned to the secondary phase of the polystyrene homopolymer.

Interestingly, the effect of accelerator on mechanical properties is considerably stronger than expected based on DMA data. Hence, the formulations treated with **Co-C** and **VO-1** exhibit considerably higher ultimate flexural strength ($\sigma_{f,max}$) and flexural modulus (E_f) than **Fe-BOC**, see Table 3. However, the excellent values of $\sigma_{f,max}$, observed for **Co-C**, came at a cost of considerably lower impact toughness (a_{cU}).

Table 3. Mechanical properties of the **PES109** formulations.

	Conc. (wt.%)	T_g,[a] (°C)	$\sigma_{f,max}$[b] (MPa)	E_f[c] (GPa)	$\varepsilon_{f,failure}$[d] (%)	a_{cU}[e] (kJ/m^2)	Gel[f] (%)
VO-1	6×10^{-4}	123.8	112.6 ± 11.1	2.53 ± 0.42	10.3 ± 1.8	19.4 ± 4.9	98.8 ± 0.1
Co-C	3×10^{-3}	125.4	128.5 ± 6.2	2.94 ± 0.34	11.1 ± 4.8	7.3 ± 2.3	98.8 ± 0.1
Fe-BOC	1×10^{-5}	130.2	52.9 ± 1.6	1.55 ± 0.10	> 15[g]	32.7 ± 5.0	97.3 ± 1.3

[a] Temperature of the glass transition determined by DMA analysis. [b] Ultimate flexural strength. [c] Flexural modulus. [d] Flexural strain at break. [e] Impact toughness. [f] Gel content. [g] Specimens did not brake upon the experiment.

3.9 Mechanical tests on polyester films

The coatings of the **PES109** formulations were prepared by casting. In this case, a higher dose of accelerators was used to prevent the inhibition of radical polymerization on the surface. The relative hardness, adhesion, and solvent resistance of post-cured coatings were investigated using a standard procedure.

VO-1 formulations exhibit excellent film hardness and good solvent resistance in the concentration range of 0.003 to 0.01 wt.% (Table 4), which is comparable to **Co-C** coatings at the optimal dose (0.01–0.03 wt.%). It corelates well with the good mechanical properties of the bulk samples mentioned above. In the case of **Fe-BOC**, considerably lower values of $H_{rel,10d}$ and $H_{rel,100d}$ were observed even at high dose (6×10^{-4} wt. %) implying a lower degree of cure.

Unfortunately, high relative hardness and good solvent resistance usually come at the cost of low adhesion, which is ascribed to the low content of the polar carboxylic and hydroxyl function groups. We note that the relative content of the polar functions increases upon undesired evaporation of styrene when the curing process is very slow. Inhibition of radical polymerization by dioxygen can also increase the content of hydroxyl groups. In this case, it appeared that peroxo species can be decomposed by accelerators and improve crosslinking of the coating. This situation probably arose at low doses of **Co-C** (0.003–0.006 wt.%), as the coatings show good adhesion but still high relative hardness.

The **PES109** formulations showed considerably lower coloration than the alkyd resins mentioned above, which is due to the lower dose of accelerators (Table 4). An increase in the yellowing index (b*) is observed only at a high dose of **Co-C.**

Table 4. Coating properties of the **PES109** formulations.

	Conc. (wt.%)	Thickness (μm)	H_{rel} [a] (%)	Adhesion [b]	Solvent Resistance [c]	L^* [d]	a^* [d]	b^* [d]
VO-1	0.01	77 ± 1	74.9	0B	4	98.3 ± 0.8	0.0 ± 0.5	1.5 ± 0.6
	0.006	62 ± 1	65.2	0B	4	98.6 ± 0.8	–0.8 ± 0.6	1.8 ± 0.2
	0.003	58 ± 2	61.7	0B	4	98.8 ± 0.4	–0.5 ± 0.1	1.7 ± 0.1
	1×10^{-3}	58 ± 1	43.6	0B	4	99.2 ± 0.5	–0.6 ± 0.3	1.4 ± 0.1
Co-C	0.03	63 ± 4	68.3	0B	4	94.1 ± 0.5	–0.9 ± 0.5	6.7 ± 0.3
	0.01	70 ± 2	57.0	0B	4	98.5 ± 0.5	–1.5 ± 0.4	4.0 ± 0.4
	0.006	69 ± 4	56.6	3B	4	98.6 ± 0.4	–1.1 ± 0.3	3.0 ± 0.3
	0.003	90 ± 2	42.6	2B	4	99.2 ± 0.8	–0.6 ± 0.6	1.4 ± 0.2
Fe-BOC	6×10^{-4}	66 ± 2	25.9	0B	4	98.9 ± 0.5	–0.7 ± 0.3	1.0 ± 0.1
	3×10^{-4}	78 ± 2	8.1	0B	4	97.9 ± 0.6	–0.3 ± 0.5	0.7 ± 0.3
	1×10^{-4}	56 ± 2	1.1	1B	2	98.6 ± 0.1	–0.4 ± 0.6	0.8 ± 0.2
	6×10^{-5}	45 ± 7	1.1	3B	1	98.6 ± 0.8	–0.5 ± 0.4	0.9 ± 0.2

[a] Relative hardness of coatings according to König. [b] Determined by cross-cut test. [c] MEK double rub resistance. [d] Coloration of the coatings in the CIELAB color space.

4. Conclusions

This study has proven that oxidovanadium(IV) dibutyl phosphate (**VO-1**) has great potential as a primary drier for alkyd paints and as an accelerator for unsaturated polyester resins. This compound is readily available on the multigram scale from common raw material using an improved synthetic protocol. The molecular structure of **VO-1** was determined by X-ray diffraction analysis. It forms an unusual trinuclear complex in the solid state, which is split on a simple mononuclear oxidovanadium(IV) species upon curing process, as evidenced by EPR spectroscopy. The strong catalytic activity of **VO-1** was documented by standard tests on several commercial alkyd binders and one multipurpose unsaturated polyester resin.

In both types of binders, the catalytic activity of **VO-1** is observed at concentrations lower than for cobalt carboxylates (**Co-2EH** and **Co-C**) but still considerably higher than in the case of **Fe-BOC**. It was shown that **VO-1** gives coatings of considerably higher hardness than **Fe-BOC**; comparable to **Co-2EH**/**Co-C**. Further mechanical tests also imply that **VO-1** behaves more like **Co-2EH**/**Co-C**. The main drawback of vanadium-based drier **VO-1** is the yellowish coloration of cured alkyd coatings. Yellowing is not observed in the case of unsaturated polyester resin due to the much lower dosage.

Authors contributions

Tomáš Foltýn prepared vanadium compounds and performed the tests on alkyd resins.

Eliška Matušková performed the test on unsaturated polyester resins.

David Rubeš contributed to the mechanical testing.

Jaromír Vinklárek supervised the project and contributed to the characterization of vanadium compounds.

Miroslava Litecká performed an X-ray analysis.

Anna Krejčová performed ICP analyses.

Jan Honzíček conceptualized the project, contributed to the characterization of the coatings, wrote the original manuscript, and edited the manuscript.

Declaration of competing interest

The authors declare that they have no known competing financial interests or personal relationships that could have appeared to influence the work reported in this paper.

Data availability

The raw data required to reproduce these findings will be made available on request.

Acknowledgements

The authors wish to acknowledge the financial support of the Faculty of Chemical Technology of the University of Pardubice (Project No. VA390018).

References

[1] L. Leyssens, B. Vinck, C. Van Der Straeten, F. Wuyts, L. Maes, Cobalt toxicity in humans - A review of the potential sources and systemic health effects, Toxicology 387 (2017) 43–56. https://doi.org/10.1016/j.tox.2017.05.015

[2] J. Briffa, E. Sinagra, R. Blundell, Heavy metal pollution in the environment and their toxicological effects on humans, Heliyon 6 (2020) e04691. https://doi.org/10.1016/j.heliyon.2020.e04691

[3] M. A. Zoroddu, J. Aaseth, G. Crisponi, S. Medici, M. Peana, V. M. Nurchi, The essential metals for humans: a brief overview, J. Inorg. Biochem. 195 (2019) 120–129. https://doi.org/10.1016/j.jinorgbio.2019.03.013

[4] J. Tang, Y. Li, X. Liu, G. Yu, F. Zheng, Z. Guo, Y. Zhang, W. Shao, S. Wu, H. Li, Cobalt induces neurodegenerative damages through impairing autophagic flux by activating hypoxia-inducible factor-1α triggered ROS overproduction, Sci. Total Environ. 857 (2023) 159432. https://doi.org/10.1016/j.scitotenv.2022.159432

[5] N. Simpson, K. Maaijen, Y. Roelofsen, R. Hage, The Evolution of Catalysis for Alkyd Coatings: Responding to Impending Cobalt Reclassification with Very Active Iron and Manganese Catalysts, Using Polydentate Nitrogen Donor Ligands, Catalysts 9 (2019) 825. https://doi.org/10.3390/catal9100825

[6] N. Supanchaiyamat, A. J. Hunt, Conservation of Critical Elements of the Periodic Table, ChemSusChem 12 (2019) 397–403. https://doi.org/10.1002/cssc.201802556

[7] M. Li, J. Lu, Cobalt in lithium-ion batteries, Science 367 (2020) 979–980. https://doi.org/10.1126/science.aba9168

[8] S. J. Bellettiere, D. M. Mahoney, Multi-Metallic Complexes: The Next Generation of Driers, J. Coat. Technol. 59 (1987) 101–108.

[9] J. Honzíček, Curing of Air-Drying Paints: A Critical Review, Ind. Eng. Chem. Res. 58 (2019) 12485–12505. https://doi.org/10.1021/acs.iecr.9b02567

[10] E. Matušková, J. Vinklárek, J. Honzíček, Effect of Accelerators on the Curing of Unsaturated Polyester Resins: Kinetic Model for Room Temperature Curing, Ind. Eng. Chem. Res. 60 (2021) 14143–14153. https://doi.org/10.1021/acs.iecr.1c02963

[11] E. Bouwman, R. van Gorkum, A study of new manganese complexes as potential driers for alkyd paints, J. Coat. Technol. Res. 4 (2007) 491–503. https://doi.org/10.1007/s11998-007-9041-0

[12] M. D. Meijer, E. van Weelde, J. T. M. Dijk, J. Flapper, Drier for auto-oxidisable coating compositions, WO Patent WO 2013/092441 A1, June 27, 2013.

[13] M. D. Meijer, E. van Weelde, J. T. M. Dijk, J. Flapper, Drier for auto-oxidisable coating compositions. WO Patent WO 2013/092442 A1, June 27, 2013.

[14] J. W. de Boer, P. V. Wesenhagen, E. C. Wenker, K. Maaijen, F. Gol, H. Gibbs, R. Hage, The Quest for Cobalt-Free Alkyd Paint Driers, Eur. J. Inorg. Chem. (2013) 3581–3591. https://doi.org/10.1002/ejic.201300205

[15] K. Wieghardt, U. Bossek, B. Nuber, J. Weiss, J. Bonvoisin, M. Corbella, S. E. Vitols, J. J. Girerd, Synthesis, Crystal Structures, Reactivity, and Magnetochemistry of a Series of Binuclear Complexes of Manganese(II), -(III), and -(IV) of Biological Relevance. The Crystal Structure of $[L'Mn^{IV}(\mu\text{-}O)_3Mn^{IV}L'](PF_6)_2\cdot H_2O$ Containing an Unprecedented Short Mn···Mn Distance of 2.296 Å, J. Am. Chem. Soc. 110 (1988) 7398–7411. https://doi.org/10.1021/ja00230a021

[16] Z. O. Oyman, W. Ming, F. Micciche, E. Oostveen, J. van Haveren, R. van der Linde, A promising environmentally-friendly manganese-based catalyst for alkyd emulsion coatings, Polymer 45 (2004) 7431–7436. https://doi.org/10.1016/j.polymer.2004.08.052

[17] Z. O. Oyman, W. Ming, R. van der Linde, Catalytic activity of a dinuclear manganese complex (MnMeTACN) on the oxidation of ethyl linoleate, Appl. Catal. A: Gen. 316 (2007) 191–196. https://doi.org/10.1016/j.apcata.2006.09.023

[18] Z. O. Oyman, W. Ming, R. van der Linde, J. ter Borg, A. Schut, J. H. Bieleman, Oxidative drying of alkyd paints catalysed by a dinuclear manganese complex (MnMeTACN), Surf. Coat. Int. B: Coat. Trans. 88 (2005) 269–275. https://doi.org/10.1007/BF02699583

[19] M. Křižan, J. Vinklárek, M. Erben, I. Císařová, J. Honzíček, Autoxidation of alkyd resins catalyzed by iron(II) bispidine complex: Drying performance and in-depth infrared study, Prog. Org. Coat. (2017) 111, 361–370. https://doi.org/10.1016/j.porgcoat.2017.05.015

[20] M. Křižan, J. Vinklárek, M. Erben, Z. Růžičková, J. Honzíček, Iron(II) complex with modified bispidine ligand: Synthesis and catalytic alkyd drying, Inorg. Chim. Acta 486 (2019) 636–641. https://doi.org/10.1016/j.ica.2018.11.035

[21] E. Matušková, J. Honzíček, Performance of Manganese(III) Acetylacetonate in Solvent-Borne and High-Solid Alkyd Formulations, Materials 13 (2020) 642. https://doi.org/10.3390/ma13030642

[22] M. Li , Y. Li , Y. Zong , Y. Song , Y. Liao , Y. Yang, Y. Zhu, Application of manganese-based driers in tung oil: drying behavior, paint film properties, and drying mechanism, Ind. Crops Prod. 206 (2023) 117733. https://doi.org/10.1016/j.indcrop.2023.117733

[23] J. Honzíček, E. Matušková, Š. Voneš, J. Vinklárek, Helmet Phthalocyaninato Iron Complex as a Primary Drier for Alkyd Paints, Materials 14 (2021) 1220. https://doi.org/10.3390/ma14051220

[24] M. Erben, D. Veselý, J. Vinklárek, J. Honzíček, Acyl-substituted ferrocenes as driers for solvent-borne alkyd paints, J. Mol. Catal. A Chem. 353–354 (2012) 13–21. https://doi.org/10.1016/j.molcata.2011.10.024

[25] J. Honzíček, T. Fedorova, J. Vinklárek, T. Mikysek, I. Císařová, Modified Ferrocenes as Primary Driers for Formulations of Alkyd Paints, Coatings 10 (2020) 873. https://doi.org/10.3390/coatings10090873

[26] J. Bootsma, W. R. Browne, J. Flapper, B. de Bruin, Photoactive Fe Catalyst for Light-Triggered Alkyd Paint Curing, JACS Au 2 (2022) 531–540. https://doi.org/10.1021/jacsau.1c00579

[27] O. Preininger, J. Honzíček, P. Kalenda, J. Vinklárek, Drying activity of oxovanadium(IV) 2-ethylhexanoate in solvent-borne alkyd paints, J. Coat. Technol. Res. 13 (2016) 479–487. https://doi.org/10.1007/s11998-015-9779-8

[28] O. Preininger, J. Vinklárek, J. Honzíček, T. Mikysek, M. Erben, A promising drying activity of environmentally friendly oxovanadium(IV) complexes in air-drying paints, Prog. Org. Coat. 88 (2015) 191–198. https://doi.org/10.1016/j.porgcoat.2015.06.026

[29] O. Preininger, I. Charamzová, J. Vinklárek, I. Císařová, J. Honzíček, Oxovanadium(IV) complexes bearing substituted pentane-2,4-dionate ligands: Synthesis, structure and drying activity in solvent-borne alkyd paints, Inorg. Chim. Acta 462 (2017) 16–22. https://doi.org/10.1016/j.ica.2017.03.008

[30] I. Charamzová, A. Machálková, J. Vinklárek, I. Císařová, J. Honzíček, Benzyl substituted oxidovanadium(IV) pentane-2,4-dionates: Synthesis, structure and drying properties, Inorg. Chim. Acta 492 (2019) 243–248. https://doi.org/10.1016/j.ica.2019.04.039

[31] I. Charamzová, J. Vinklárek, P. Kalenda, I. Císařová, J. Honzíček, Oxidovanadium(V) dithiocarbamates as driers for alkyd binders, J. Coat. Technol. Res. 17 (2020) 1113–1122. https://doi.org/10.1007/s11998-020-00326-3

[32] M. Klussmann, N. J. Simpson, J. Honzicek, P. Kalenda, J. Vinklarek, I. Charamzova, Paints Containing Driers on Vanadium Compounds Bearing Anions of Sulfonic Acids as Counter Ions, WO Patent WO 2021/260037 A1, December 31, 2021.

[33] N. J. Simpson, M. Klussmann, J. Halstead, S. Brand, Paints Containing Driers Based on Vanadium Compounds Bearing Various Acid Anions, WO Patent WO 2023/117421 A1, June 29, 2023.

[34] R. F. Toorkey, K. C. Rajanna, P. K. S. Prakash, Curing of Unsaturated Polyester: Network Formation, J. Chem. Educ. 73 (1996) 372–373. https://doi.org/10.1021/ed073p372

[35] J. F. G. A. Jansen, I. Hilker, E. Kleuskens, G. Hensen, I. Kraeger, W. Posthumus, Cobalt Replacement in Unsaturated Polyester Resins; Going for Sustainable Composites, Macromol. Symp. 329 (2013) 142–149. https://doi.org/10.1002/masy.201200102

[36] J. F. G. A. Jansen, R. I. Kraeger, Unsaturated Polyester Resin Compositions, WO Patent WO 2008/003500 A1, January 10, 2008.

[37] G. Link, D. Edelmann, E. Stumpp, Verwendung spezieller Vanadiumverbindungen als Sikkative für oxidativ trochnende Lacke, European patent EP 0870811 A2, October 14, 1998.

[38] G. Link, D. Edelmann, E. Stumpp, Use of Special Vanadium Compounds as Siccatives for Oxidatively Drying Lacquers, US patent US 6063841 A, May 16, 2000.

[39] A. L. Harold, Process for curing unsaturated polyesters using a vanadium compound and an acid phosphate ester as catalysts. US patent US 3238274 A, March 1, 1966.

[40] CrysAlisPRO, Version 1.0.43; Rigaku Oxford Diffraction: Yarnton, UK, 2022.

[41] O. V. Dolomanov, L. J. Bourhis, R. J. Gildea, J. A. K. Howard, H. Puschmann, OLEX2: a complete structure solution, refinement and analysis program, J. Appl. Crystallogr. 42 (2009) 339–341. https://doi.org/10.1107/S0021889808042726

[42] G. M. Sheldrick, SHELXT - Integrated space-group and crystal-structure determination, Acta Crystalogr. A 71 (2015) 3–8. https://doi.org/10.1107/S2053273314026370

[43] G.M. Sheldrick, Crystal structure refinement with SHELXL, Acta Crystallogr. C 71 (2015) 3–8. https://doi.org/10.1107/S2053229614024218

[44] ASTM D5895-20. Standard Test Methods for Evaluating Drying or Curing During Film Formation of Organic Coatings Using Mechanical Recorders; ASTM International: West Conshohocken, PA, USA, 2020.

[45] ISO 2535:2001. Plastics-Unsaturated Polyester Resins-Measurement of Gel Time at Ambient Temperature; International Organization for Standardization: Genèva, Switzerland, 2001.

[46] D. Rubeš, J. Vinklárek, L. Prokůpek, Š. Podzimek, J. Honzíček, Styrene-free unsaturated polyester resins derived from itaconic acid curable by cobalt-free accelerators, J. Mater. Sci. 58 (2023) 6203–6219. https://doi.org/10.1007/s10853-023-08407-5

[47] ISO 1522:2006. Paints and Varnishes. Pendulum Damping Test; International Organization for Standardization: Genève, Switzerland, 2007.

[48] ISO 2808:2007. Paints and Varnishes. Determination of Film Thickness; International Organization for Standardization: Genève, Switzerland, 2007.

[49] ASTM D4752-98. Standard Practice for Measuring MEK Resistance of Ethyl Silicate (Inorganic) Zinc-Rich Primers by Solvent Rub; ASTM International: West Conshohocken, PA, USA, 1998.

[50] ASTM D3359-17. Standard Test Methods for Rating Adhesion by Tape Test; ASTM International: West Conshohocken, PA, USA, 2017.

[51] ASTM D1708-18. Standard test method for tensile properties of plastics by use of microtensile specimens. ASTM International: West Conshohocken, PA, USA, 2018.

[52] ISO 178:2019. Plastics. Determination of flexural properties. International Organization for Standardization: Genève, Switzerland, 2019.

[53] ČSN 64 0612. Plastics. Determination of charpy impact properties; Czech Office for Standards, Metrology and Testing, Czech Republic, 1982.

[54] I. Charamzová, J. Vinklárek, J. Honzíček, Effect of primary driers on oxidative drying of high-solid alkyd binder: Investigation of thickness effects by mechanical tests and infrared spectroscopy, Prog. Org. Coat. 125 (2018) 177–185. https://doi.org/10.1016/j.porgcoat.2018.09.001

[55] N. Herron, D. L. Thorn, R. L. Harlow, G. W. Coulston, Molecular Precursors to Vanadyl Pyrophosphate and Vanadyl Phosphite, J. Am. Chem. Soc. 119 (1997) 7149–7150. https://doi.org/10.1021/ja970179m

[56] M. Sato, T. Takayanagi, Y. Fujita, T. Kwan, Electron-spin-resonance Studies of the Formation and Properties of the trimeric Vanadyl Dibutylphosphate Complex, Bull. Chem. Soc. Japan 46 (1973) 727–736. https://doi.org/10.1246/bcsj.46.727

[57] J. S. Maass, Z. Chen, M. Zeller, F. Tuna, R. E. P. Winpenny, R. L. Luck, Syntheses, X-ray Structural Characterizations, and Thermal Stabilities of Two Nonclassical Trinuclear Vanadium(IV) Complexes, $(V_3(\mu_3\text{-}O)O_2)(\mu_2\text{-}O_2P(CH_2C_6H_5)_2)_6(H_2O)$ and $(V_3(\mu_3\text{-}O)O_2)(\mu_2\text{-}O_2P(CH_2C_6H_5)_2)_6(py)$, and Polymeric Complexes of Stoichiometry $(VO(O_2PR_2)_2)_\infty$, R_2 = Ph_2 and *o*-$(CH_2)_2(C_6H_4)$, Inorg. Chem. 51 (2012) 2766−2776. https://doi.org/10.1021/ic201259u

[58] J. S. Maass, Z. Chen, M. Zeller, R. L. Luck, Syntheses and characterization of the vanadium trimer $(V_3(\mu_3\text{-}O)O_2)(\mu_2\text{-}O_2P(CH_2C_6H_5)_2)_6$(4,4'-bipyridine) and the vanadium hexamer $[(V_3(\mu_3\text{-}O)O_2)(\mu_2\text{-}O_2P(CH_2C_6H_5)_2)_6]_2(\mu_2\text{-}N^1,N^2$-di(pyridin-4-yl)oxalamide), J. Coord. Chem. 69 (2016) 2342–2352. https://doi.org/10.1080/00958972.2016.1188383

[59] Rostiashvili, V. G.; Vilgis, T. A. Statistical Thermodynamics of Polymeric Networks. In *Encyclopedia of Polymeric Nanomaterials*. Springer-Verlag: Berlin, Heidelberg, 2014.